Applied Catalysis B: Environmental 156–157 (2014) 456–465

Contents lists available at ScienceDirect

Applied Catalysis B: Environmental

journal homepage: www.elsevier.com/locate/apcatb

Microwave-enhanced degradation of phenol over Ni-loaded ZnO nanorods catalyst

Aseel Bala Ahmed[a,1], Baba Jibril[a,*], Supamas Danwittayakul[b], Joydeep Dutta[c,*]

[a] Petroleum and Chemical Engineering Department, Sultan Qaboos University, PO Box 33, Al Khoudh, PC 123, Muscat, Oman
[b] National Metal and Materials Technology Center, 114 Thailand Science Park, Klong Nueng, Klong Luang, Tha Khlong 12120, Pathumthani, Thailand
[c] Chair in Nanotechnology, Water Research Center, Sultan Qaboos University, PO Box 33, 123, Al-Khoudh, Muscat, Oman

ARTICLE INFO

Article history:
Received 23 November 2013
Received in revised form 17 February 2014
Accepted 18 March 2014
Available online 27 March 2014

Keywords:
Phenol degradation
ZnO nanorods
Ni/ZnO nanocatalyst
Wastewater treatment

ABSTRACT

Nickel was loaded onto hydrothermally-grown ZnO nanorods on cordierite substrates and tested as catalysts in microwave-enhanced degradation of phenol from its aqueous solution (100 ppm) at 70 °C. Effects of metal loadings (1, 10 and 20 mM impregnation solutions) on the degradation of phenol in aqueous solution was investigated. The catalyst performances were monitored based on phenol degradation, product distributions and carbon dioxide (CO_2) evolutions. Based on the type of the catalysts, two different mechanistic pathways for the decomposition were observed—through catechol and/or hydroquinone as intermediates. It was found that the 10 mM nickel loaded sample catalyzed the degradation through one pathway with hydroquinone as the benzenediol intermediate formed, while the 20 mM nickel impregnated sample catalyzed the reaction through two pathways, producing catechol as well as hydroquinone by products. These differences in reaction pathways were attributed to the variation in the composition of the nickel compounds and surface structures between the two catalysts. Furthermore, the effect of hydrogen peroxide (H_2O_2) as an oxidant was explored. It was found that although addition of H_2O_2 led to an increase in the degree of phenol degradation, it also led to enhanced catalyst leaching. There was also an increase in CO_2 evolution due to the addition of H_2O_2. It was observed that 20 mM nickel-loaded sample without the addition of H_2O_2 exhibited optimum performance in terms of phenol degradation and CO_2 evolution with no drawback of catalyst leaching. Catalytic microwave enhanced degradation is an effective means for the removal of dissolved organic compounds from wastewater.

1. Introduction

With the rise of industrialization around the world and tightening of water quality regulations, the effective treatment of wastewater has become a greater challenge. This has led to increasing interest in the research of enhanced technologies for the removal of hazardous pollutants. Because of its use and manufacture in many industries including refineries, coal processing and petrochemicals, phenol is omnipresent in wastewater. As a highly toxic contaminant at even small concentrations with low biodegradability, phenol contamination of water is considered a hazard to human health. In addition to this, the oxidation of numerous higher molecular weight compounds produces phenol as an intermediate compound. These characteristics make phenol a widely used model pollutant in the study of wastewater treatment technologies [1–5]. The removal of phenol from wastewater has been reported using a variety of techniques including photocatalysis [6–13], electrical discharge [14,15] and catalytic wet air oxidation [1,16,17]. Microwave-enhanced oxidation has gained recent attention [18–20] because it provides a more uniform thermal environment than conventional heating. This effectively leads to higher reaction rates, shorter reaction times and greater energy efficiency. This is because microwave interacts directly with dipole molecules such as water and phenol. Such interaction leads to rotational movement of the molecules based on the respective frequencies. Therefore, microwave is used to directly heat the phenol aqueous solution without heat transfer from the heating element to the system as in the conventional heating mechanisms.

Other agents used to enhance phenol degradation are oxidants and catalysts. The addition of an oxidant, such as hydrogen

* Corresponding authors at: Sultan Qaboos University, Petroleum and Chemical Engineering, Alkhoud 123, Muscat, Oman. Tel.: +968 24142582; fax: +968 513416.
E-mail addresses: baba@squ.edu.om (B. Jibril), dutta@squ.edu.om (J. Dutta).
[1] Present address: Department of Chemical Engineering and Material Science, Michigan State University, East Lansing, MI, USA.

http://dx.doi.org/10.1016/j.apcatb.2014.03.032
0926-3373/

peroxide, enhances mineralization rate of phenol due to the increase in the concentration of hydroxyl radicals [4,21]. However, treatment with H_2O_2 also has its drawbacks. Several studies have shown that, up to a certain extent, an increasing concentration of H_2O_2 enhances the extraction of metals such as nickel from the catalysts [22,23]. This is a major disadvantage in wastewater treatment as it necessitates the inclusion of a downstream separation unit to remove leached metals from treated water, an option which is often physically or economically unfeasible [17,24]. In addition to this, H_2O_2 must be transported and stored with care because of its tendency to disintegrate into water and oxygen. The chemical is also an eye, skin and lung irritant and forms an explosive mixture with organic compounds. For these reasons, substituting H_2O_2 in oxidation processes with a catalyst of equal or greater efficiency is of utmost interest.

The efficiency of a catalyst is dependent on a number of factors including its surface area, morphology and surface chemistry. It is well-established that the growth of nanostructures such as nanorods on a surface enhances its surface area significantly [25]. The loading of these nanostructures with active species enhances the reactivity of the surface. Metal oxides, especially those of transition metals such as nickel, have been found to significantly increase the oxidation process [20,26]. In the present study, catalysts were produced by enhancing an inert cordierite substrate with ZnO nanorods and loading different quantities of nickel onto the surface. These were characterized and the effect of loading on the phenol degradation was investigated using UV–vis, infrared and mass spectroscopy. Results were then compared to those of similar experiments conducted under the same conditions with the addition of hydrogen peroxide.

2. Experimental

2.1. Preparation of Ni/ZnO catalyst

For catalyst synthesis, all chemicals were of analytical grade and used as received without further purification. These consisted of: ethanol (C_2H_5OH), zinc acetate dihydrate ($Zn(CH_3COO)_2{\cdot}2H_2O$) and zinc nitrate hexahydrate ($Zn(NO_3)_2{\cdot}6H_2O$) from Merck, hexamethylene tetramine (hexamine: $C_6H_{12}N_4$) from Sigma-Aldrich, and nickel(II) acetate ($Ni(CH_3COO)_2$) from Univar.

ZnO nanorods were grown on porous cordierite ceramic substrates (consisting of magnesium iron aluminum cyclosilicate procured from Zhongtian Co. Ltd., China) through a hydrothermal technique described in detail elsewhere [27]. Surface impurities on the cordierite honeycomb substrate were removed by washing with ethanol in an ultrasonic bath for 5 min. The substrate was seeded by immersing it into a 2 mM zinc acetate in ethanol solution and then boiling off the solvent at temperatures above 350 °C in air. This was done 10 times to obtain uniform distribution of ZnO nanoparticles on the substrates.

Hydrothermal processing was conducted in a bath of zinc nitrate hexahydrate and hexamethylene tetramine (5 mM each) at 95 °C for up to 15 h in order to epitaxially grow ZnO nanorods on the substrate [25,28]. The ZnO nanorods on ceramic substrates were then annealed at 350 °C for 1 h.

Further processing involved in-situ precipitation to impregnate the ZnO nanorods grown on the cordierite substrates with Ni^{2+} ion precursors. The ZnO substrates were dipped into 1, 10 and 20 mM nickel acetate solutions in deionized water at room temperature (25 °C) for 1 h. The samples were then washed rigorously and calcined at 350 °C for 1 h to decompose acetate compound to produce the metal nanoparticles. Based on the concentrations of nickel precursor solution, the catalyst samples are referred to as 1, 10 and 20 mM Ni loading.

2.2. Characterization of Ni/ZnO catalyst

Microstructure of the catalysts were investigated in a field emission scanning electron microscope (JEOL JSM-5410) operating at 20 kV equipped with an energy dispersive spectroscopy (EDS) detector after coating with platinum to minimize charging effects. A JEOL JEM-2010 field emission electron transmission microscope operating at 200 kV was used to investigate nanostructure of the catalysts.

X-ray diffraction (XRD) patterns were collected using Rigaku MiniFlex600 at 40 kV, 15 mA and a scanning speed and step size of 10 deg/min and 0.02°, respectively, for 2θ values from 3 to 90°. To find the relative surface area, a 1000 ppm suspension of each catalyst in deionized water was prepared and inserted into a particle surface area analyzer (Xigo Nanotools Acorn Area). In the nuclear magnetic resonance (NMR) relaxation measurement by the Xigo nanotools system, a magnetic field perturbation is induced. The corresponding response of the hydrogen nuclei in the sample is then detected. For a static field at equilibrium, the spin magnetic moments of these nuclei align with the field. The spins can be excited to higher energy levels by applying a pulse. As the spins relax to equilibrium, the nuclear magnetization is observed [29]. The NMR relaxation consists of longitudinal relaxation time T_1, defining the decay of spin alignment and the transverse relaxation time T_2, defining the decay of precession. Although T_1 measurements are more common in the literature, they are more time consuming than T_2 measurements using Carr–Purcell–Meiboom–Gill (CPMG) method [30]. NMR transverse relaxation (T_2) of fluids confined in a porous material is affected by pore surface, by the bulk relaxation process in the fluid and additionally by dephasing in case of molecular diffusion. Bulk relaxation (T_{2Bulk}) is significantly smaller than the surface relaxation and so where relaxation of diffusion ($T_{2Diffusion}$) is slow, the relaxation ($1/T_2$) may be related to surface relaxivity (ρ_p) and surface to volume ratio of pores (S_p). The estimation of surface area (SA) measurement by NMR relaxation method is possible as bound liquid in contact with a particle surface has a relaxation rate significantly different from that of free liquid. The surface area is related to the relaxation by Eq. (1)

$$R_{av} = \psi_p SL\rho_p (R_b - R_f) + R_f \quad (1)$$

where ψ_p represents the ratio of volume of particles to the volume of liquid, S is the surface area per unit weight, L is the thickness of surface layer of fluid and ρ_p is the bulk density of particles. R_b, the relaxation rate constant of the bound liquid and R_f, the relaxation rate constant of the free liquid is determined from the spin relaxation time, T_1 or T_2. The layer thickness, L is assumed constant with particle size. For an unknown material, it is necessary to obtain an independent estimate of bulk relaxation, R_b and in our case we assumed the bulk relaxation in ZnO.

2.3. Phenol degradation

To prepare for the degradation studies, 30 ml of 100 ppm aqueous phenol solution was placed in a teflon lined vessel and the solution pH was adjusted to 7 ± 0.1 using dilute sodium hydroxide and hydrochloric acid. 2 mg of catalyst and, for runs with hydrogen peroxide, 9 ml of 15 mM H_2O_2 were added to the aqueous phenol solution. In both cases, a control was run where no catalyst was included. The vessel was then inserted into a Milestone Start D Microwave Digestion System operating at 750 W that heated the samples from room temperature to 70 °C in 5 min. This temperature

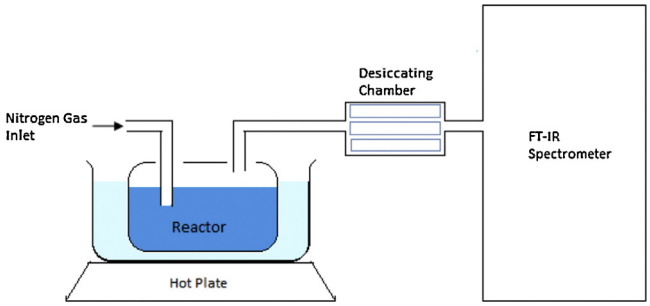

Fig. 1. Experimental Set-up for evolved gas analysis to detect CO_2 during the degradation of phenol with catalysts and/or H_2O_2.

was maintained for 2 min and then the samples were left to cool down to room temperature.

A Perkin Elmer Lambda 25 UV/vis Spectrophotometer was used to analyze the phenol and treated solutions in the wavelength region of 200–700 nm at a scanning speed and slit width of 480 nm/min and 1 nm, respectively. In addition to this, the mass spectra in positive polarity was obtained using a Micromass Quattro Ultima Pt Mass Spectrometer. The operating condition of mass spectrometer is provided as follows: 70 scans were accumulated at a cycle time of 250 ms with an interscan delay of 100 ms. Electrospray ionizations were carried out and a mass range of 50–200 amu was collected for each sample.

2.4. Measurement of evolved CO_2

An experiment was designed to investigate the evolution of CO_2 from the degradation of phenol using the Ni/ZnO catalysts. The experimental setup is shown in Fig. 1.

At the start of each experiment, the feed gas line and the spectrometer were purged with nitrogen gas (99.999% purity) for 10 min in order to remove any atmospheric carbon dioxide and moisture; a background with nitrogen gas was then recorded. Following this, phenol solution with additives (catalyst and/or hydrogen peroxide) in the same quantities and concentrations, mentioned earlier, was heated in a water bath for approximately 5 min to 70 °C. Upon reaching this temperature, the gases evolved from the reactions were guided to a Perkin Elmer FT-IR Frontier Spectrometer through a desiccating chamber (to remove water vapor) using a steady flow rate of nitrogen gas. The spectrometer was operated at a resolution of 4 cm^{-1} and the infrared spectra from 400 to 4000 cm^{-1} was collected every 6 s for 30 min at constant temperature.

3. Results and discussion

3.1. Characterization of Ni/ZnO catalyst

Fig. 2 shows the Scanning electron micrographs (SEM) and corresponding energy dispersive spectra (EDS) obtained for catalysts with 1 (Fig. 2i), 10 (Fig. 2ii) and 20 mM (Fig. 2iii) nickel loading. For all catalyst samples, the elements in the cordierite substrate (magnesium, aluminum, iron and silicon) as well as the Zinc (Zn) from the zinc oxide nanorods are observed in the EDS. The nickel loading in the 1 mM Ni loaded catalyst (Fig. 2i) appeared to be below the limit of the detector and was thus not observed. However, for the 10 and 20 mM Ni loaded catalysts (Fig. 2ii and iii), the nickel peaks are clearly visible, indicating the presence of higher quantities of nickel in the samples.

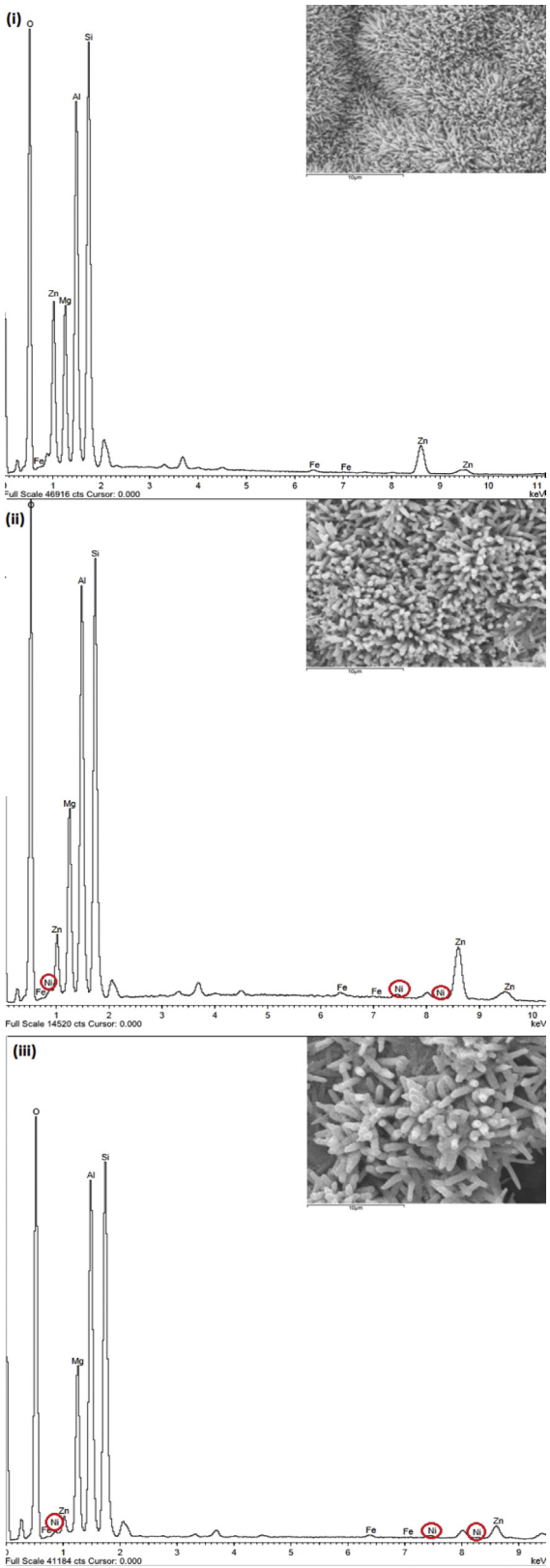

Fig. 2. EDS graphs and SEM images generated by (i) 1 mM, (ii) 10 mM and (iii) 20 mM nickel loaded catalyst.

In the case of 1 mM Ni loaded catalyst, dense and slender 120–200 nm diameter ZnO nanorods were observed (Fig. 2i). Ni deposition is hardly visible in the low resolution SEM but are clearly observed in the High Resolution transmission electron micrograph

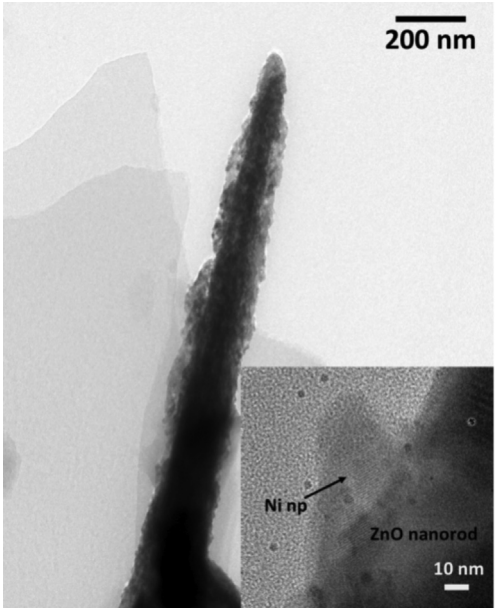

Fig. 3. Transmission electron micrograph of a typical ZnO nanorod loaded with Ni nanoparticles deposited at 1 mM concentration.

(HRTEM) as shown in Fig. 3. In this typical micrograph we can observe ZnO nanorod decorated with about 30 nm Ni particles. The 10 mM Ni loaded catalysts were found to be cover by Ni (NiO, $Ni(OH)_2$) nanoparticles with thicker ZnO nanorods that appear to have a lower length over width ratio (200–320 nm rods width) (Fig. 2ii). This is an indication that some disintegration and subsequent redeposition of the ZnO rods during the impregnation with Ni ions may have occurred. The effects of this phenomenon are more apparent in the SEM micrograph of 20 mM Ni loaded catalyst where thicker nanorods (about 500–700 nm width) with nanofibrous network structure of Ni–ZnO catalyst was observed [27].

X-ray diffraction (XRD) patterns for the catalysts in the region where cordierite peaks do not mask the ZnO, Ni and nickel oxide peaks are shown in Fig. 4 for 1, 10 and 20 mM nickel loaded catalysts. The complete XRD spectra are given in Supp. Fig. 1 for reference.

For 2θ values below 70°, the peaks of the cordierite substrate mask all other diffraction peaks as cordierite is the major component of the catalysts. However, for 2θ values between 70 and 90°, diffraction patterns for zinc, zinc oxide, nickel, nickel oxide and nickel hydroxide are clearly distinguishable. For the 1 mM nickel loaded catalyst, the intensity due to nickel is lower than that of the other two catalysts. For 10 and 20 mM nickel loaded catalysts, peaks for nickel and nickel compounds become more apparent. To gain insight into the nature of phases in the catalyst, a quantitative analysis using reference intensity ratio (RIR) method was conducted on the XRD diffraction pattern as shown in Fig. 5.

As can be observed, nickel in the form of compounds or in its metallic form in the 1 mM Ni catalyst are more evenly distributed than in the case of the other two catalysts. At 50%, NiO is identified as the primary nickel compound on the 1 mM Ni loaded catalyst. When 10 mM nickel loading was used, formation of $Ni(OH)_2$ far exceeds that of NiO. In addition to this, the percentage of NiO formed is approximately half of what was observed for the 1 mM Ni catalyst. In the case of the 20 mM nickel loaded catalyst, the portion of $Ni(OH)_2$ formed is even greater than on the 10 mM Ni loaded catalyst and less of the other nickel compounds were observed.

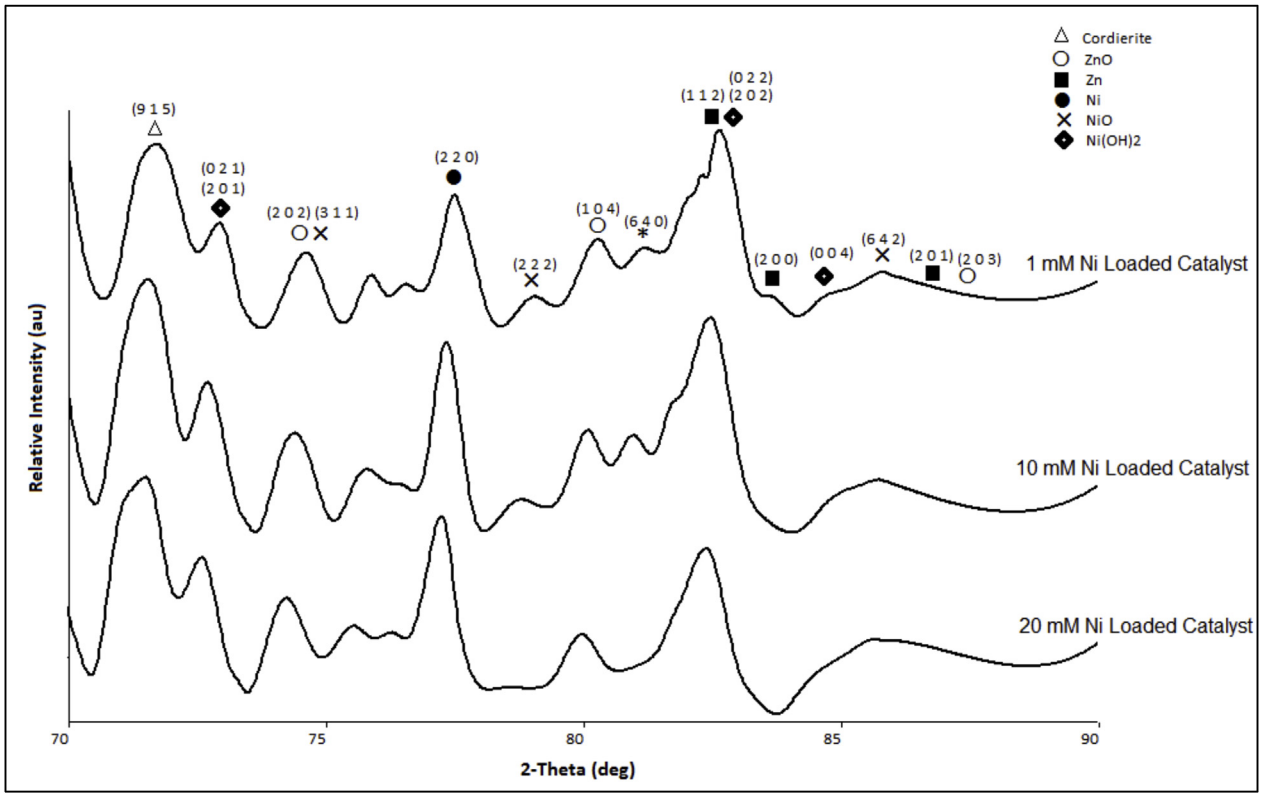

Fig. 4. XRD diffraction patterns for 1, 10 and 20 mM nickel loaded catalysts.

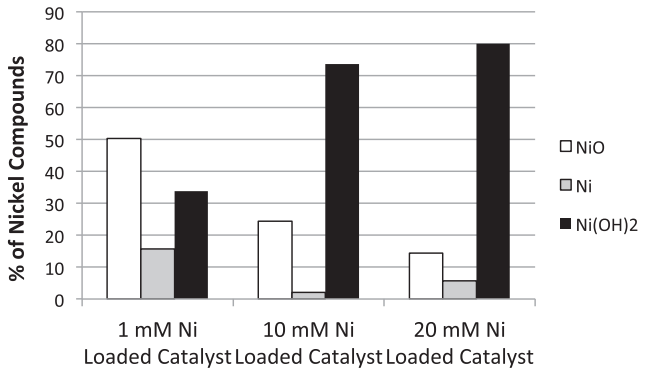

Fig. 5. Distribution of nickel compounds on 1, 10 and 20 mM nickel loaded catalysts based on a quantitative analysis of the XRD diffraction patterns (using RIR method).

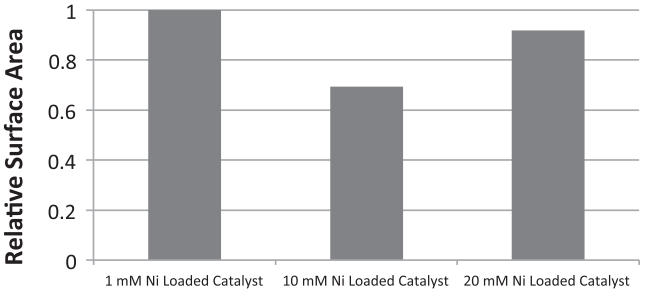

Fig. 6. Relative surface area of 1, 10 and 20 mM nickel loaded catalysts.

To gain a more comprehensive understanding of the catalyst surfaces, the relative surface areas were determined and are presented in Fig. 6 for 1, 10 and 20 mM nickel loaded catalysts. It can be observed that the catalyst with the least amount of nickel loading has the largest surface area. In comparison, the surface area exhibited by the 10 mM Ni loaded catalyst is significantly smaller. The 20 mM Ni loaded catalyst has the second highest surface area. This trend in surface area is in agreement with the SEM micrographs discussed earlier depicting long ZnO rods for the 1 mM Ni loaded catalyst, shorter rods for the 10 mM Ni loaded catalyst (due to the early stages of ZnO dissolution) and microballs on the surface of the 20 mM Ni loaded catalyst (due to extensive dissolution and redeposition) [28].

3.2. Phenol degradation

In Fig. 7, the optical absorption band of phenol in an aqueous solution is compared to those of phenol treated in a microwave reactor for 2 min at 70 °C and 1 atm pressure without a catalyst, and with 1 mM, 10 mM and 20 mM nickel loaded catalyst. The sole absorption peak observed for all spectra occurred at 270 nm (complete spectra is given in Supp. Fig. 2). When the phenol was treated in a microwave reactor, a reduction in peak absorbance of phenol could be observed (Fig. 7ii). The absorbance was further reduced when the 10 mM nickel loaded catalyst was added to the phenol sample during the microwave treatment. However, when 1 or 20 mM nickel loaded catalyst were used, the absorption peak was found to increase. UV absorption of intermediates could be the cause of the higher optical absorption in the sample treated with 20 mM nickel loaded catalyst. In order to better comprehend the phenol degradation process, the mass spectra of the samples were collected and analyzed.

Fig. 8i shows the obtained mass spectra of the phenol in reaction products after microwave treatment without any catalysts. The spectra give percentage distribution of the products. The relevant products are shown in the figure. Intermediate products including methylfurfuryl alcohol and short-chain lighter compounds such as isobutene, hydroxy-acetic acid and 3-(vinyloxy)propene with no significant absorbance bands at 270 nm could be detected. Thus, the observed UV peak is purely an indication of the decreased phenol concentration in the solution. However, the mass spectra of subsequent samples treated in the presence of catalysts revealed the creation of heavier molecules.

In the case of the 1 mM nickel loaded catalyst, the first stages of bond breakage and recombination become apparent as larger compounds are formed. Based on the mass spectra shown in Fig. 8ii and the rise in the UV absorbance band discussed earlier, maleic acid could be one of the major byproducts. When the precursor concentration was increased tenfold, almost all compounds produced had mid-range molecular weights (between 94 and 150 g/mol). Fig. 8iii shows that the phenol concentration was reduced to its

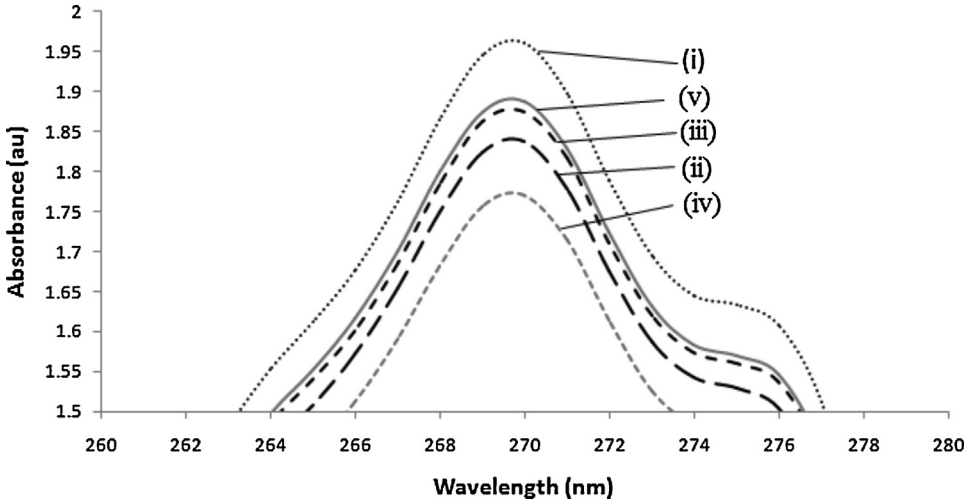

Fig. 7. UV spectra for (i) phenol and phenol treated in a microwave reactor for 2 min at 70 °C under atmospheric pressure with (ii) no catalyst, (iii) 1 mM, (iv) 10 mM and (v) 20 mM nickel loaded catalyst.

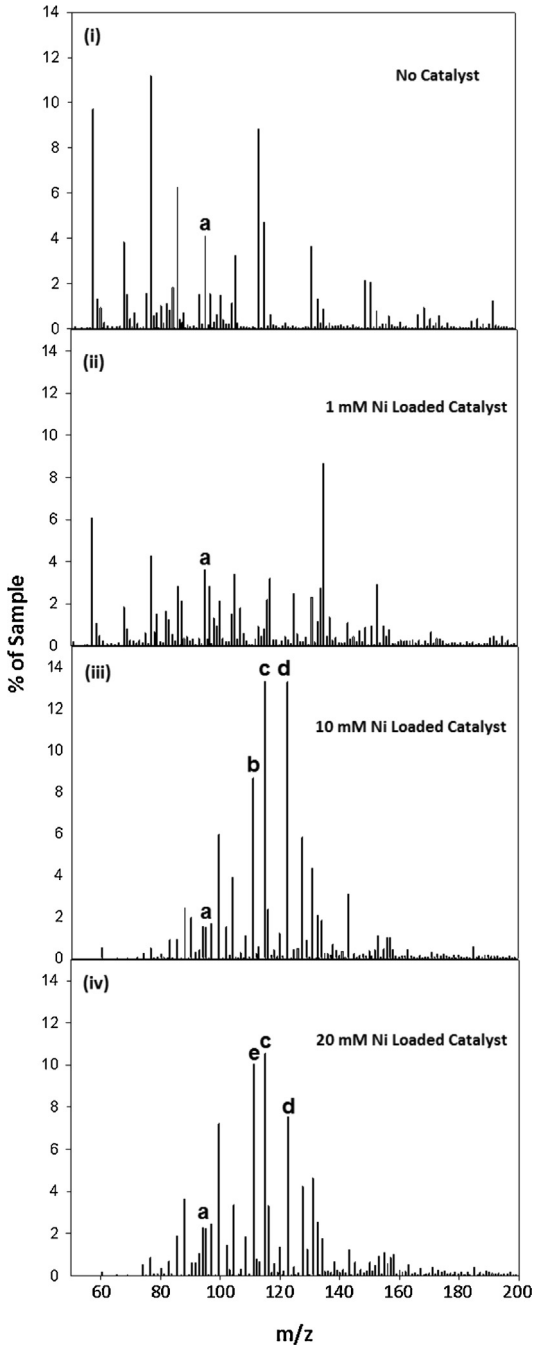

Fig. 8. Mass Spectra for phenol treated in a microwave reactor for 2 min at 70 °C under atmospheric pressure with no catalyst, 1 mM, 10 mM and 20 mM nickel loaded catalyst where (a) phenol, (b) hydroquinone, (c) maleic/fumaric acid, (d) methyl-*p*-benzoquinone, (e) catechol.

lowest and fewer compounds could be observed with only three compounds accounting for more than 50% of the solution. The measured molar masses of these compounds indicate that they are benzenediol, butenedioic acid (maleic or fumaric acid) and a third compound that is likely to be methyl-*p*-benzoquinone or hydroxybenzoic aldehyde. In order to identify the benzenediol isomer, the differences in the absorbance spectra of catechol and hydroquinone were used. It has been found that the presence of catechol reduces the rate of degradation of other phenolic compounds due to the interference of catechol with OH^- [31]. This interaction not only inhibits the deactivation of H_2O_2 (as given by Eq. (2)) but also impedes the regeneration of hydroxl groups from air.

$$H_2O_2 + {}^{\bullet}OH \rightarrow H_2O + HO_2{}^{\bullet} \quad (2)$$

Due to significantly lower optical absorption of the sample treated in oven in the presence of 10 mM nickel loaded catalyst compared to other samples described here, it implies that hydroquinone is the benzenediol being generated, as catechol shows an optical absorption at 270 nm that would lead to a higher optical absorption peak (Fig. 7), which was not observed. This characteristic of catechol was also used to identify it as the benzenediol produced in the 20 mM nickel loaded catalyst sample. Apart from this exception, the mass spectrum produced by the run yielded similar results to those observed in the samples treated with 10 mM nickel loaded catalyst.

Based on the presence of hydroquinone, methyl-*p*-benzoquinone and butenedioic acid, a reaction pathway can be determined. It is proposed that the phenol first undergoes hydroxylation where it is broken down primarily to hydroquinone. It is further oxidized to yield *p*-benzoquinone, short-chain acids and eventually carbon dioxide. Accelerated by the higher surface area and increased $Ni(OH)_2$ concentration of the 20 mM nickel loaded catalyst discussed earlier, a secondary pathway takes precedence through which phenol is hydroxylated to catechol and gets eventually oxidized to carbon dioxide as shown in Fig. 9. These intermediates are very similar to those reported by Santos et al. [3] for phenol oxidation over copper catalyst in acidic medium. It is further proposed that the main reason for the change in the primary degradation pathway between the 10 and 20 mM catalyst is the increase in the $Ni(OH)_2$ available in the 20 mM loaded catalyst. Lipczynska-Kochany [32] studied the flash pyrolysis of phenol treated with H_2O_2 and reported that the ortho-hydroxylation of the phenol aromatic ring takes precedence leading to the increased production of catechol. Alnaizy et al. [33] reported a catechol to hydroquinone ratio greater than one in the degradation of phenol using advanced oxidation process with hydrogen peroxide and nickel catalysts. A similar trend was followed in the case of the 20 mM nickel loaded catalyst.

In another study by Lai et al. [20], the microwave degradation of phenol on nickel oxide catalyst (mix-valenced and NiO_x calcined at 300, 400 and 500 °C) was investigated and it was found that the only observable intermediate was malonic acid. This indicates that the mechanism of phenol breakdown was through the hydroquinone path. For the 10 mM nickel loaded catalyst under study, the identification of hydroquinone as the main benzenediol isomer suggests a similar reaction mechanistic pathway as that reported by Lai et al. [20] The lack of oxalic acid in the mass spectra of all phenol solution samples indicates that the secondary reaction pathway has gone to completion, producing carbon dioxide and water.

As mentioned before, the addition of hydrogen peroxide to a phenol solution accelerated mineralization. In order to gauge the effect of an oxidant addition compared to the catalysts, a similar study was carried out in which hydrogen peroxide was added to the phenol solution during treatment in the microwave reactor.

Fig. 10 shows the UV spectra of an aqueous phenol solution mixed with hydrogen peroxide compared to the same solution after treatment in the microwave reactor for 2 min at 70 °C and 1 atm without catalyst, and with the three nickel loaded catalysts. The optical absorption peaks of treated samples were found to be below that of the untreated phenol and H_2O_2 solution. It can be observed that, with the introduction of the 1 and 10 mM nickel loaded catalyst, the optical absorbance peak reduced even further. Yet, similar to observations reported earlier (in the absence of H_2O_2),

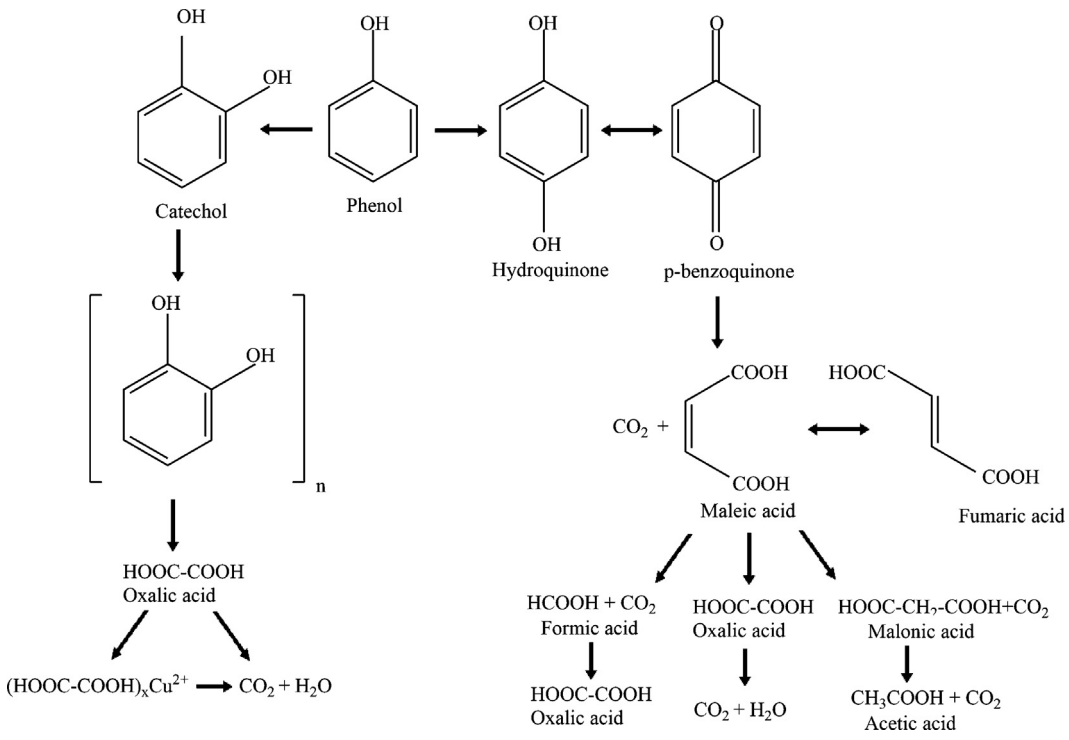

Fig. 9. Phenol oxidation pathway in aqueous phase with copper catalyst as proposed by Santos et al.

when the 20 mM loaded catalyst was used, the peak intensity increased.

Mass spectra of the samples were analyzed to verify the composition of the liquid solution and the results can be seen in Fig. 11.

With the addition of hydrogen peroxide, Zn, NiO and $Ni(OH)_2$ are detected in the mass spectra of the solutions. As this result is unique to solutions treated with H_2O_2, it can be deduced that the hydroxyl radicals initiated a leaching process from the catalyst. It can be observed that NiO quantities increase with catalyst loading for the cases of 1 mM and 10 mM loaded catalyst (10 mM catalyst > 1 mM catalyst). However, for the 20 mM catalyst the quantity of NiO decreases and that of $Ni(OH)_2$ becomes significantly greater than in the first two cases. This is most likely due to nickel compound distribution on the 20 mM loaded catalyst discussed earlier. Leaching of nickel oxide catalysts has been reported by Alejandre et al. [34] in their study of nickel and copper nickel catalysts in the phenol degradation. It was found that the metal leaching into the phenol solution during degradation enhanced homogeneous catalytic reactions in degradation. These reactions primarily produce

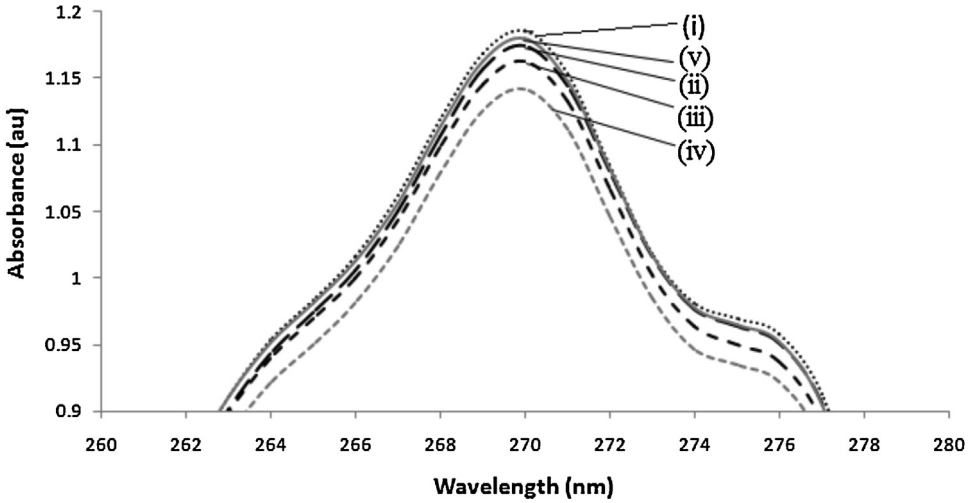

Fig. 10. UV spectra for (i) phenol and phenol treated in a microwave reactor for 2 min at 70 °C under atmospheric pressure with H_2O_2 and (ii) no catalyst, (iii) 1 mM, (iv) 10 mM and (v) 20 mM nickel loaded catalyst.

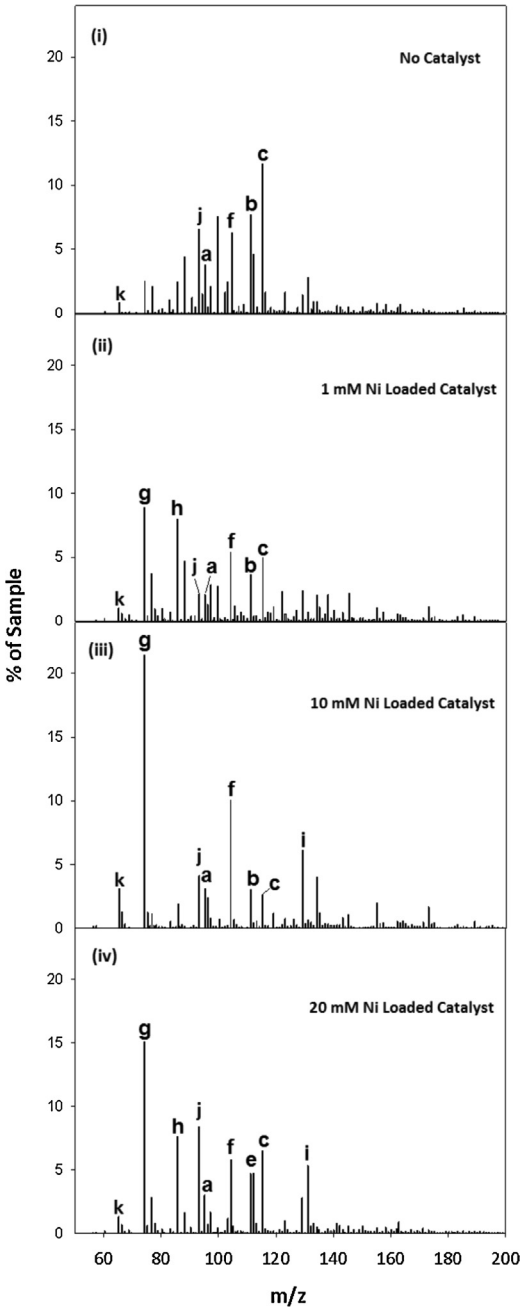

Fig. 11. Mass Spectra for phenol treated in a microwave reactor with H_2O_2 for 2 min at 70 °C under atmospheric pressure with no catalyst, 1 mM, 10 mM and 20 mM nickel loaded catalyst where (a) phenol, (b) hydroquinone, (c) maleic/fumaric acid, (e) catechol, (f) malonic acid, (g) NiO, (h) phenol fragment, (i) hydroxybenzoic aldehyde (j) $Ni(OH)_2$ and (k) Zn.

polymers and decrease total phenol oxidation [26,35]. Similar to results reported by Alejandre [34] and Pintar [35], no significant polymerization products were identified in the mass spectra. It can therefore be concluded that the contribution of homogeneous catalysis in the present study is much less than that of heterogeneous catalysis. However, as mentioned earlier, the presence of metal compounds in the solution necessitates the addition of further separation units downstream, the feasibility of homogeneous catalysis should be evaluated at an early stage of the process design.

It can be observed from Fig. 11 that when phenol was heated by microwave without a catalyst, the majority of the phenol was converted to hydroquinone, butenedioic and malonic acid. With the addition of 1 mM loaded catalyst, twice as much phenol was converted and more of the butenedioic acid oxidized to malonic acid. It is proposed that this is because the reaction path is close to completion, producing malonic acid and gaseous CO_2. The 10 mM nickel loaded sample catalyzes the reaction closer to completion as evident by an increase in malonic acid concentration. When the catalyst loading was doubled, a similar phenomena to that of the corresponding case with no hydrogen peroxide occurs. The UV peak rise indicates that the hydroxylation pathway to catechol was also present.

According to the pathway presented in Fig. 9, the presence of malonic acid as a major byproduct of phenol degradation in the presence of H_2O_2 indicates that the final product would be acetic acid. It is more desirable to accelerate the pathway leading to carbon dioxide and water as final product. Because only one reaction pathway is detected with the 10 mM nickel loaded catalyst whereas both are observed with the 20 mM nickel loaded catalyst, the carbon dioxide evolved from the latter should be significantly higher. In order to verify this, a separate experiment was designed to detect the amount of CO_2 evolved from the phenol solution while it was heated in the presence of the catalyst and/or H_2O_2.

Fig. 12 shows the FTIR spectra produced by heating phenol solutions with five different additive combinations at 70 °C over time (complete spectra is available in Supp. Fig. 3). It can be observed that an absorbance peak occurs at 2360 cm^{-1} for all runs which corresponds to the asymmetric stretching of carbon dioxide.

Fig. 13 shows the CO_2 IR absorption peak produced by the phenol solution after 2 min of irradiation in the microwave reactor with five additive combinations: only hydrogen peroxide, 10 mM nickel loaded catalyst, H_2O_2 and 10 mM nickel loaded catalyst, 20 mM nickel loaded catalyst and H_2O_2 and 20 mM nickel loaded catalyst. It can be observed that, when only H_2O_2 is added to the phenol solution, an evolution of carbon dioxide is detectable. However, the amount of CO_2 generated was almost doubled when 10 mM nickel loaded catalyst was used without any H_2O_2. Combining these two additives produces an even greater CO_2 absorbance peak. When the 20 mM nickel loaded catalyst was used, the CO_2 absorbance peak was found to be more than 2.5 times higher than that generated by the phenol samples treated in the microwave reactor with only H_2O_2. When the 20 mM nickel loaded catalyst and hydrogen peroxide were used in conjunction, the IR peak generated for CO_2 was approximately the same as that produced with only 20 mM loaded catalyst. Hydrogen peroxide did not significantly enhance CO_2 production in this case. The catalyst efficiency (in terms of CO_2 evolution) for 10 mM loading is about 100% above the values without the catalyst. The values increased to 153% for 20 mM loading sample.

It can be observed that in both cases with and without H_2O_2, the 20 mM nickel loaded catalyst produces significantly higher quantities of carbon dioxide than the 10 mM nickel loaded catalyst. For this increase in CO_2 generation to occur, the phenol degradation in the presence of 20 mM nickel loaded catalyst must be activating the secondary pathway to completion, producing carbon dioxide as a final product. A time graph of CO_2 evolution (Fig. 14) was generated by monitoring changes in the 2306 cm^{-1} peak over a period of 1 h. Production of CO_2 gradually increased over time as the temperature was ramped up from room temperature to 70 °C and then became constant as thermal stability was reached. This verifies that the gas detected during the course of the experiment was generated in the reactor.

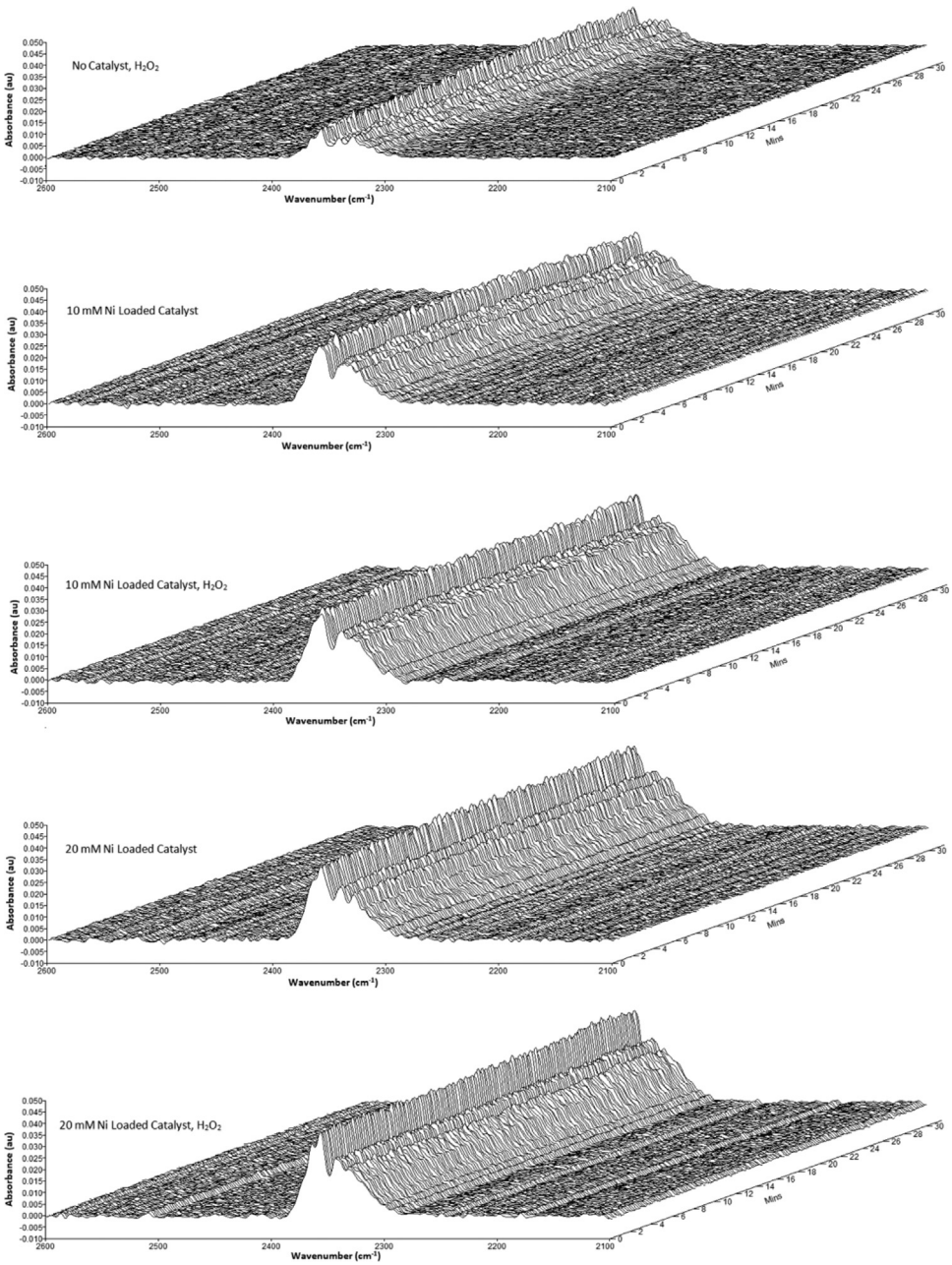

Fig. 12. CO_2 IR peak (2306 cm^{-1}) detected during heating at 70 °C for five different catalyst/H_2O_2 additive combinations.

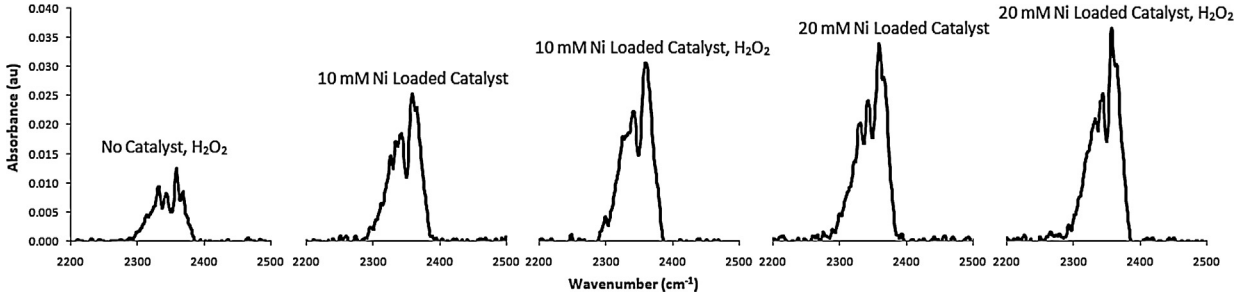

Fig. 13. CO_2 IR peak (2306 cm^{-1}) detected after 2 min of heating at 70 °C for five different catalyst/H_2O_2 additive combinations.

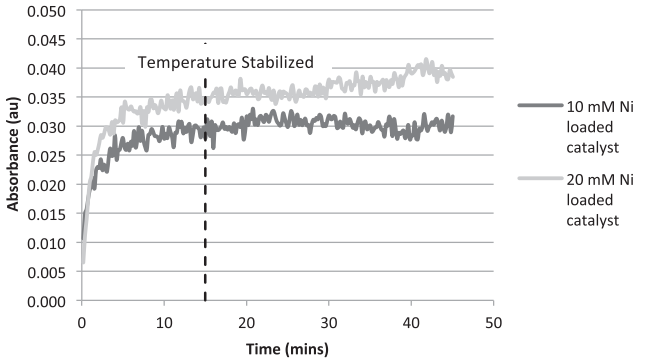

Fig. 14. Carbon dioxide peak fluctuations over time with 10 mM and 20 mM Ni loaded catalyst (with H_2O_2).

4. Conclusions

Cordierite substrates enhanced with ZnO rods were successfully impregnated with different concentrations of Ni and the activities of the resulting catalysts on the degradation of phenol were studied. It was observed that with increased nickel loading (10 and 20 mM), disintegration and redeposition of the ZnO nanorods occurs whereby the rods become thicker and shorter. It was found that, catalysts of different loadings (10 vs. 20 mM Nickel) enhanced the degradation via different mechanistic pathways. Sample with 10 mM Ni loaded catalysts led to the formation of hydroquinone as the benzenediol intermediate, while the 20 mM Ni loaded catalyst exhibited two pathways, with the possibility of production of both hydroquinone and catechol. Consequently, a greater evolution of carbon dioxide was expected for the case of the 20 mM nickel loaded catalyst and this was proved in a separate CO_2 detection experiment. It is proposed that the initiation of the second decomposition pathway in the case of the 20 mM nickel loaded sample is due to the higher concentration of $Ni(OH)_2$ and greater surface area than the 10 mM nickel loaded catalyst. Furthermore, the effect of addition of H_2O_2 as an oxidant was explored. Results were then compared to similar experiments run with hydrogen peroxide. In the latter case, phenol was found to decompose into malonic acid, indicating a final product of acetic acid and carbon dioxide. In addition to this, significant leaching of Zn, NiO and $Ni(OH)_2$ from the catalysts occurred. Although H_2O_2 may enhance the degradation reaction, the leaching poses important challenge.

Acknowledgments

AB would like to gratefully acknowledge the financial support received from Sultan Qaboos University, The Research Council and the Chair in Nanotechnology for carrying out this work. We would also like to thank the staff of SQU's colleges of science, engineering and medicine laboratories for their assistance and contribution.

Appendix A. Supplementary data

Supplementary data associated with this article can be found, in the online version, at http://dx.doi.org/10.1016/j.apcatb.2014.03.032.

References

[1] S. Zhou, Z. Qian, T. Sun, J. Xu, C. Xia, Appl. Clay Sci. 53 (2011) 627–633.
[2] P.S. Suchithra, C.P. Shadiya, A. Peer Mohamed, P. Velusamy, S. Ananthakumar, Appl. Catal., B: Environ. 53 (44) (2013) 130–131.
[3] A. Santos, P. Yustos, A. Quintanilla, S. Rodríguez, F. García-Ochoa, Appl. Catal., B: Environ. 39 (2002) 97–113.
[4] B. Jibril, A. Atta, Y. Al-Waheibi, T. Al-Waheibi, J. Ind. Eng. Chem. 19 (6) (2013) 1800–1804.
[5] Y. Liu, Y. Zhu, J. Xu, X. Bai, R. Zong, Y. Zhu, Appl. Catal., B: Environ. 142–143 (2013) 561–567.
[6] J. Araña, E. Tello Rendón, J.M. Doña Rodrı′guez, J.A. Herrera Melián, O. González Dı′az, J. Pérez Peña, Appl. Catal., B: Environ. 30 (2001) 1–10.
[7] J. Araña, E. Pulido Melián, V.M. Rodríguez López, A. Peña Alonso, J.M. Doña Rodríguez, O. González Díaz, J. Pérez Peña, J. Hazard. Mater. 146 (2007) 520–528.
[8] K.M. Parida, S. Parija, Sol. Energy 80 (2006) 1048–1054.
[9] J.F. Montoya, J.A. Velásquez, P. Salvador, Appl. Catal., B: Environ. 88 (2009) 50–58.
[10] K. Naeem, F. Ouyang, J. Environ. Sci. 25 (2) (2013) 399–404.
[11] S. Valencia, F. Cataño, L. Rios, G. Restrepo, J. Marín, Appl. Catal., B: Environ. 104 (2011) 300–304.
[12] S.-H. Lin, C.-H. Chiou, C.-K. Chang, R.-S. Juang, J. Environ. Manage. 92 (2011) 3098–3104.
[13] M.H.M.T. Assumpção, R.F.B. De Souza, R.M. Reis, R.S. Rocha, J.R. Steter, P. Hammer, I. Gaubeur, M.L. Calegaro, M.R.V. Lanza, M.C. Santos, Appl. Catal., B: Environ. 142–143 (2013) 479–486.
[14] Y. Shen, L. Lei, X. Zhang, M. Zhou, Y. Zhang, J. Hazard. Mater. 150 (2008) 713–722.
[15] H. Kušić, N. Koprivanac, B. Locke, J. Hazard. Mater. 125 (2005) 190–200.
[16] A. Quintanilla, J.A. Casas, A.F. Mohedano, J.J. Rodríguez, Appl. Catal., B: Environ. 67 (2006) 206–216.
[17] A. Santos, P. Yustos, A. Quintanilla, F. García-Ochoa, Chem. Eng. Sci. 60 (2005) 4866–4878.
[18] X. Bi, P. Wang, H. Jiang, X. Huan-yan, S. Shu-jie, H. Jun-li, J. Environ. Sci. 19 (2007) 1510–1515.
[19] X. Bi, P. Wang, H. Jiang, J. Hazard. Mater. 154 (2008) 543–549.
[20] T.-H. Lai, C.-C. Lee, K.-S. Wu, Y.-Y. Shu, C.-B. Wang, Appl. Catal., B: Environ. 68 (2006) 147–153.
[21] R. Prucek, M. Hermanek, R. Zbořil, Appl. Catal., A: Gen. 366 (2009) 325–332.
[22] W. Mulak, A. Szymczycha-Madeja, A. Lésniewicz, W. Zyrnicki, Physicochem. Probl. Miner. Process. 40 (2006) 69–76.
[23] E. David, J. Achiev. Mater. Manuf. Eng. 25 (1) (2007) 15–18.
[24] M. Saeed, M. Ilyas, Appl. Catal., B: Environ. 129 (2013) 247–254.
[25] S. Danwittayakul, J. Dutta, Int. J. Hydrogen Energy 37 (2012) 5518–5526.
[26] J. Levec, A. Pintar, Catal. Today 124 (2007) 172–184.
[27] S. Danwittayakul, J. Dutta, J. Alloys Compd. 586 (2014) 169–175.
[28] S. Danwittayakul, J. Dutta, Chem. Eng. J. 223 (2013) 304–308.
[29] E. Grunewald, R. Knight, Geophysics 76 (4) (2011) G73–G83.
[30] Y.H. Carr, E.M. Purcell, Phys. Rev. 94 (1954) 630.
[31] J. Araña, V.M. Rodríguez López, E. Pulido Melián, M.I. Suárez Reyes, J.M. Doña Rodríguez, O. González Díaz, Catal. Today 129 (1–2) (2007) 177–184.
[32] E. Lipczynska-Kochany, Environ. Pollut. 80 (2) (1993) 147–152.
[33] R. Alnaizy, A. Akgerman, Adv. Environ. Res. 4 (2000) 233–244.
[34] A. Alejandre, F. Medina, P. Salagre, A. Fabregat, J.E. Sueiras, Appl. Catal., B: Environ. 18 (1998) 307–315.
[35] A. Pintar, G. Bercic, J. Batista, J. Levec, Stud. Surf. Sci. Catal. 110 (1997) 633–642.